Journal of Achievements in Materials and Manufacturing Engineering
VOLUME 41
ISSUES 1-2
July-August
2010

Influence of geometry of rapidly solidified rods on properties of Fe-Co-based alloy

S. Lesz*, S. Griner, R. Nowosielski
Division of Nanocrystalline and Functional Materials and Sustainable Pro-ecological Technologies, Institute of Engineering Materials and Biomaterials,
Silesian University of Technology, ul. Konarskiego 18a, 44-100 Gliwice, Poland
* Corresponding author: E-mail address: sabina.lesz@polsl.pll

Received 21.04.2010; published in revised form 01.07.2010

Materials

ABSTRACT

Purpose: The main aim of the paper was investigation of influence of geometry of rapid solidified rods on properties (structure, fracture morphology, microhardness) of $Fe_{36}Co_{36}B_{19}Si_5Nb_4$ alloy.
Design/methodology/approach: The following experimental techniques were used: differential thermal analysis (DTA), scanning electron microscopy (SEM), light microscopy (LM), X-ray diffraction (XRD) method, Vickers microhardness.
Findings: Changes of mechanical properties (microhardness) and different fracture morphology of rapidly solidified rods were presented.
Research limitations/implications: Obtained structures are depended on cooling rate and glass forming ability of the alloy.
Practical implications: The rapidly solidified bulk alloys have been commercialized in magnetic application and high strength materials.
Originality/value: Diverse fracture morphology as well as changes of microhardness in amorphous regions of differently relaxated rate are observed.
Keywords: Amorphous materials; Fracture morphology; Microhardness; XRD, SEM and LM method

Reference to this paper should be given in the following way:
S. Lesz, S. Griner, R. Nowosielski, Influence of geometry of rapidly solidified rods on properties of Fe-Co-based alloy, Journal of Achievements in Materials and Manufacturing Engineering 41/1-2 (2010) 16-25.

1. Introduction

Fe-based amorphous alloy ribbons are one of the major soft magnetic materials, because of their superior magnetic properties such as the relatively high saturation magnetization and good magnetic softness [1-10]. However, the preparation of the ordinary amorphous magnetic alloys requires cooling rates higher than 10^4 K/s due to the low glass-forming ability (GFA) and thus restricts the material outer shape. Recently, Fe-Co-metalloid-based bulk metallic glasses (BMGs) have been developed because of their attractive properties, such as low hysteresis losses under cyclic magnetic excitation, as well as high mechanical strength combined with good ductility and good deformability in the supercooled liquid region. These alloys have relatively high GFA, leading to the formation of BMG rod with diameters of mm-order prepared by Cu mold casting with much lower cooling rates than that of the melt-spinning used for the production of amorphous alloy thin ribbons without glass transition [11].

Amorphous alloys are thermodynamically unstable and have a tendency to transit to crystals when the temperature is higher than the crystallization temperature, T_x. Even when the temperature is lower than T_x, their structures may also be changed to some extent because of the structure relaxation. The relaxation mechanisms can be divided into reversible and irreversible types. Reversible

relaxation seems to be associated with changes in the chemical short range order, while the irreversible relaxation seems to be associated with changes in the topological short range order. In addition, during structural relaxation, the density of an alloy increases and changes occur in many properties. Changes properties because of crystallization and structure relaxation may restrict their applications. Thus investigation on the thermal stability of amorphous alloys is very important and a lot of efforts have been made [12, 13].

Although much is known about the crystallization and structural relaxation of amorphous alloys induced by annealing [2, 12,] as well as their effects on the properties, little work on expansion behavior and its correlation to structure relaxation of bulk amorphous alloys have been done.

In this paper, the influence of geometry of rapid solidified rods on properties (structure, fracture morphology, microhardness) of $Fe_{36}Co_{36}B_{19}Si_5Nb_4$ alloy is studied.

2. Experiments

Investigations were carried out on bulk metallic glass in rods form with compositions of $Fe_{36}Co_{36}B_{19}Si_5Nb_4$. The Fe-based master alloy ingots with above compositions were prepared by arc melting the pure Fe, Co, Nb metals and non-metallic elements: Si, B, in an argon atmosphere. The alloy compositions represent nominal atomic percentages. The master alloy was melted in a quartz crucible using an induction coil. Each ingot was re-melted at least few times, in order to ensure the chemical homogeneity. Melting liquid was eject to split mould with two different form: square and circular. From the master alloy, rods with square section 1.5 and 2.5 mm as well as diameter with 3.0 and 5.0 mm were prepared by an ejection copper mold casting method.

Thermal properties (liquidus -T_l and solidus - T_s temperatures of the pre-alloyed ingots upon heating and cooling were analyzed by a NETZSCH model DSC 404 C Pegasus under the purified argon atmosphere, at the heating and cooling rate of 20 K/min.

The microstructure of the rods was examined by X-ray diffraction (XRD) and light microscopy method (LM).

The X-ray method has been performed by the use of diffractometer XRD 7, Seifert-FPM firm, with filtered Co-Kα radiation. X-ray diffraction patterns of the were performed from surface and core of rods with 3.0 and 5.0 mm in diameter but rods with smaller diameter were powdered for measurements. These obtained powder represented average phase composition of sample.

In order to conduct structural study, the light microscope LEICA MEF 4A in the range of 100× to 1000× magnitude was used. In addition, one rod with 5 mm in diameter on the etched cross-sectional surface was examined by means of the scanning electron microscope (SEM) SUPRA 25, ZEISS firm.

The morphology of fracture surfaces after decohesion was observed in SEM.

Microhardness was measured with a use of the Vickers hardness tester FUTURE-TECH FM-700 under a load of 0.49N (50G) [14].

3. Results and discussion

The DTA curve of the base master alloy under the heating shows two endothermic peaks (Fig. 1). The first peak for base alloy begins near the eutectic (melting) point – T_e =1201 K. The maximum signal of the second peak is separate and occurs at temperature 1353 and 1368 K . This signal is associated with the liquidus temperature T_l [15]. Such DTA traces under the heating is connected with transit of hardsoluble crystalline phases into the liquid state.

Only one major peak is observed in Fig 1 - DTA curves of the base master alloy under the cooling. This peak is undoubtedly the crystallization temperature and the maximum signal of the peak occurs at temperature1262 K. This peak is the eutectic transformation temperature and indicated that chemical composition of investigated alloy was correct chosen. From DTA analysis the onset of solidification occurs at 1268 K and end at 1213 K. The onset of solidification corresponds to the eutectic temperature T_e (Fig. 1) [15].

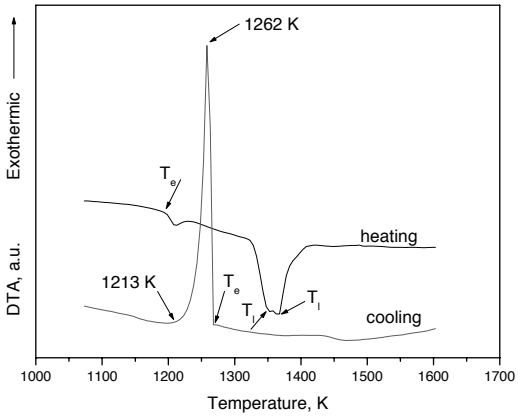

Fig. 1. Differential thermal analysis (DTA) curves of the base master alloy under the heating/cooling rate of 20 K/min

It was found from the obtained results of structural studies performed by X-ray diffraction that diffraction pattern of surface as well as powdered rods with 1.5 mm in diameter of $Fe_{36}Co_{36}B_{19}Si_5Nb_4$ alloy consists of a broad-angle peak (Fig. 2). This peak correspond with the Bragg line originating from amorphous phase of alloy on the basis of Fe-Co.

For surface of rod with 2.5 mm in diameter, the X-ray diffraction shows a broad diffraction, which is typical for the amorphous phase. The phase composition of surface is different from the phase composition of powdered rod with 2.5 mm in diameter (Fig. 3). Structure of powdered material from the rod with 2.5 mm diameter beside the amorphous phase consist of crystalline phases. Identification of these phase allow to presume, that there are (Fe,Co)α , CoB, FeB, Fe_2B, Co_2B, Co_3B, $Fe_3(Si, B)$, $Fe_{23}B_6$ phases (Fig. 3).

It was found from the transverse cross-sectional structure of the $Fe_{36}Co_{36}B_{19}Si_5Nb_4$ rods with diameter of 1.5 and 2.5 mm studies performed by light microscopy (LM) was smooth and has metallic luster (Fig. 4a,b), similar to the report [16]. Smooth

surface of the copper mould enables easy removal of the rods after solidification.

Existence of the precipitated fine-crystalline phases has been identified in core of the rod (Fig. 6), causes that on X-ray diffraction pattern is composed of a broad diffusion background and a set of several sharp crystalline peaks (Fig. 3).

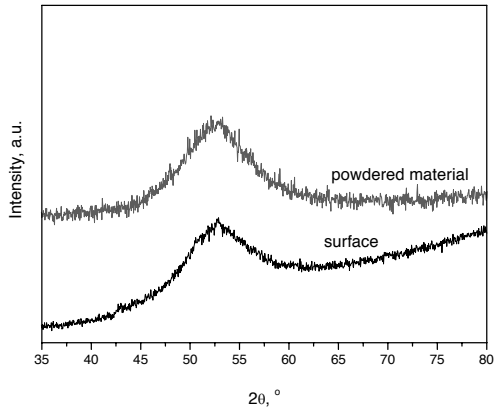

Fig. 2. X-ray diffraction pattern taken from the surface and from the powdered material of the $Fe_{36}Co_{36}B_{19}Si_5Nb_4$ rods with 1.5 mm in diameter

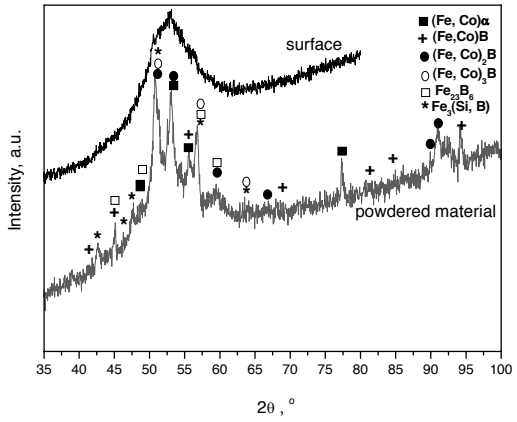

Fig. 3. X-ray diffraction pattern taken from the surface and from the powdered material of the $Fe_{36}Co_{36}B_{19}Si_5Nb_4$ rods with 2.5 mm in diameter

It was found from the obtained results of structural studies performed by X-ray diffraction, that structure of the surface and the transverse cross sections of the $Fe_{36}Co_{36}B_{19}Si_5Nb_4$ rod with 3.0 mm in diameter is clearly different (Fig. 5). On X-ray diffraction pattern for the transverse cross sections of the rod with 3.0 mm in diameter, existence of sharp crystalline peak originating from crystalline (Fe,Co)α phase in place of broad diffraction maxima typical for the amorphous phase was stated (Fig. 5). Weak peaks appear in Fig. 5 also indicate the existence of (Fe,Co)α phase.

The $Fe_{36}Co_{36}B_{19}Si_5Nb_4$ rod with 3.0 mm in diameter have different structure on surface, in core and in transition zone (Fig. 7). After etched the different microstructure zones were exposed (A, B, C in Fig. 7).

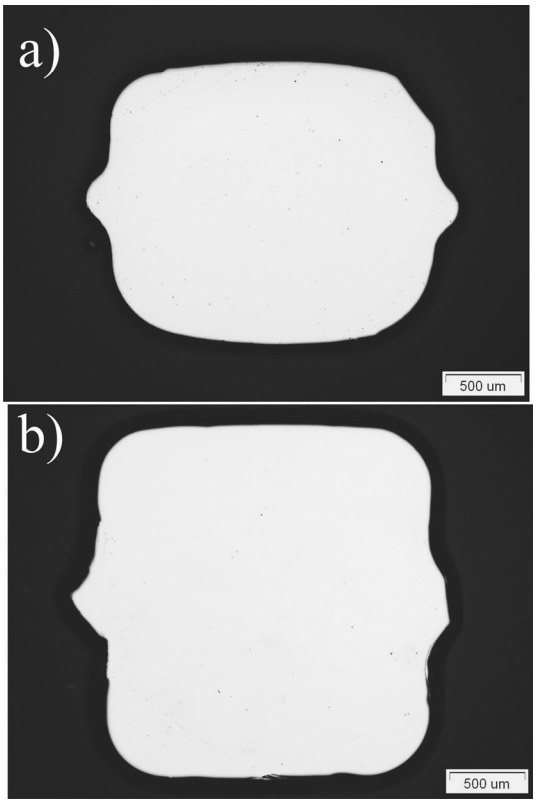

Fig. 4. Optical micrographs of the transverse cross sections of the $Fe_{36}Co_{36}B_{19}Si_5Nb_4$ rods with 1.5 mm (a) and 2.0 mm (b) in diameter

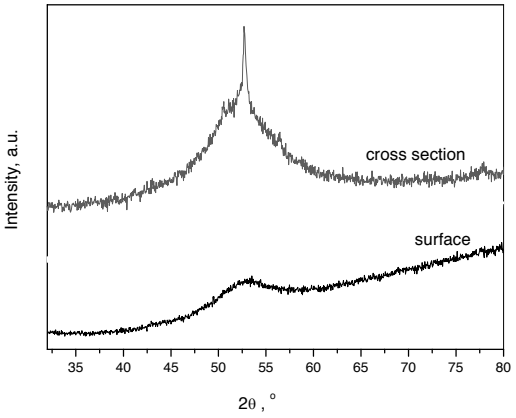

Fig. 5. X-ray diffraction pattern taken from the surface and from the cross section of the $Fe_{36}Co_{36}B_{19}Si_5Nb_4$ rods with 3.0 mm in diameter

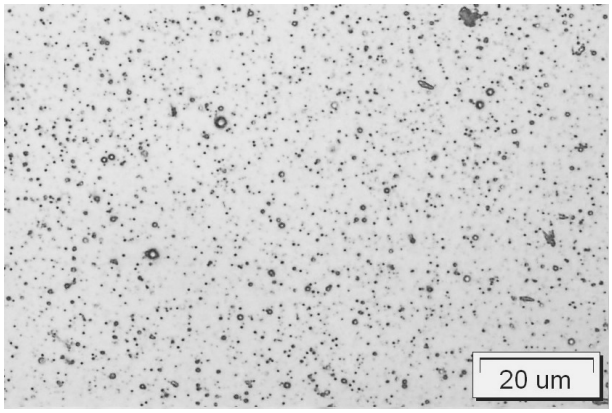

Fig. 6. Optical micrographs of the transverse cross sections after etching of the core of the $Fe_{36}Co_{36}B_{19}Si_5Nb_4$ rods with 2.0 mm in diameter

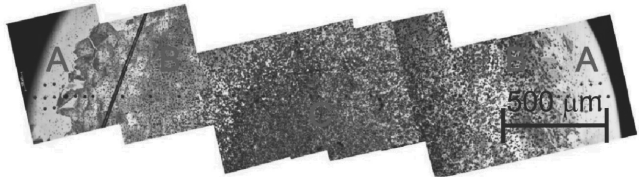

Fig. 7. Optical micrographs of the transverse cross sections after etching of the $Fe_{36}Co_{36}B_{19}Si_5Nb_4$ rods with 3.0 mm in diameter; A - zone having contact with the copper mould during cooling, B - zone - region between surface and core of rod, C - zone - core of rod

On the sample's edge, zone having contact with the copper mould during cooling (A- zone) occurs in homogenous light-etched zone (Fig. 7). B - zone region between surface and core of rod was etched on transitional colour. However C- zone, core of rod, was etched on dark colour (Fig. 7). Clearly visible crystalline phase with 5 - 10 µm grain size in this zone ware observed (Fig.8).

The X-ray tests prove that the structure of surface and core of rod with 5.0 mm in diameter (Fig. 9) is similar to structure of powdered material of rod with 2.5 mm in diameter (Fig. 3). The crystalline phases of the $Fe_{36}Co_{36}B_{19}Si_5Nb_4$ rod with 5.0 mm in diameter are identified as a: (Fe, Co)α, CoB, FeB, Fe_2B, Co_2B, Co_3B, Fe_3B, $Fe_3(Si, B)$, $Fe_{23}B_6$ (Fig. 9). The XRD pattern taken from the surface of rods with 5 mm in diameter shows a broad-angle peak, indicated that the existence of small amount of amorphous phase (Fig. 9). From comparison of the obtained X-ray diffraction patterns follows that contribution and type of individual phases is somewhat different on the surface and in the core of the rod (Fig. 9).

Results of LM and SEM investigations confirmed existence of amorphous phase in structure of the rod (Figs. 10 a, 11).

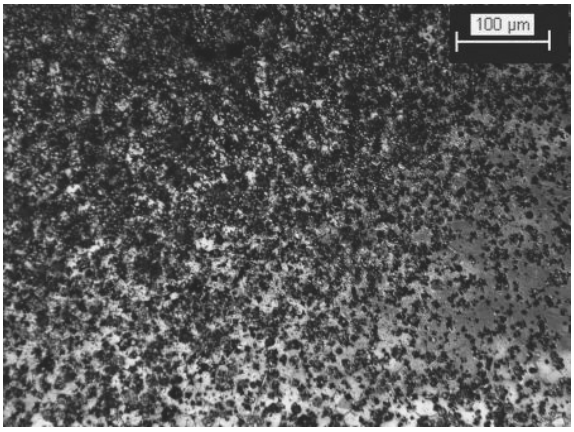

Fig. 8. Optical micrographs of the transverse cross sections after etching of the core of the $Fe_{36}Co_{36}B_{19}Si_5Nb_4$ rods with 3.0 mm in diameter

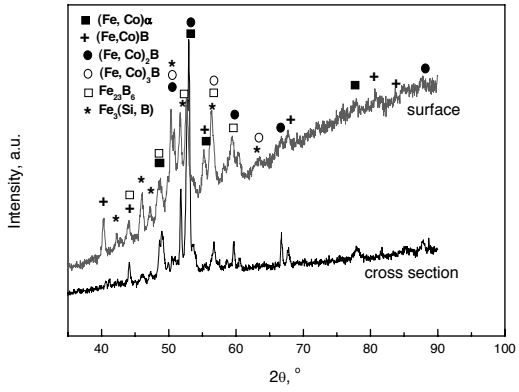

Fig. 9. X-ray diffraction pattern taken from the surface and from the cross section of the $Fe_{36}Co_{36}B_{19}Si_5Nb_4$ rods with 5.0 mm in diameter

In zone of surface of rod light etched zone corresponds with the amorphous phase (Figs. 10a, 11). In zone of core and of transition zone occur crystalline phases with spherical morphology (B-zone in Fig. 10 a, Fig. 10b), acicular (B and C-zone in Fig. 10 a, Fig. 10c) and dendritic, partially visible like a rosace crystallities growing from one nucleus of crystallization (C-zone in Fig 10a, Fig. 10 c).

Microanalysis of chemical composition of surface of rod with 5.0 mm in diameter, examined by scanning electron microscope (SEM), shows existence of elements of alloy with a composition Fe=38.18, Co=39.49, Si=6.63%, Nb=4.63 at.% (Fig. 11). Results of SEM method confirm existence of crystalline phases. beside the amorphous phase (Fig. 11).

In core of the rod occur (Fe,Co)α phase (Fig. 12, 13 I) and regions with typical form for the crystalline eutectic (Fig. 12, 13III) with increase Si and Nb concentration (Si=12.97%, Nb=9.76%) and precipitations Nb enriched (Fig. 13II.) and homogeneously disperse crystalline phases with dendritic form (Fig. 12). Similar phases to the observed was shown in ref. [17].

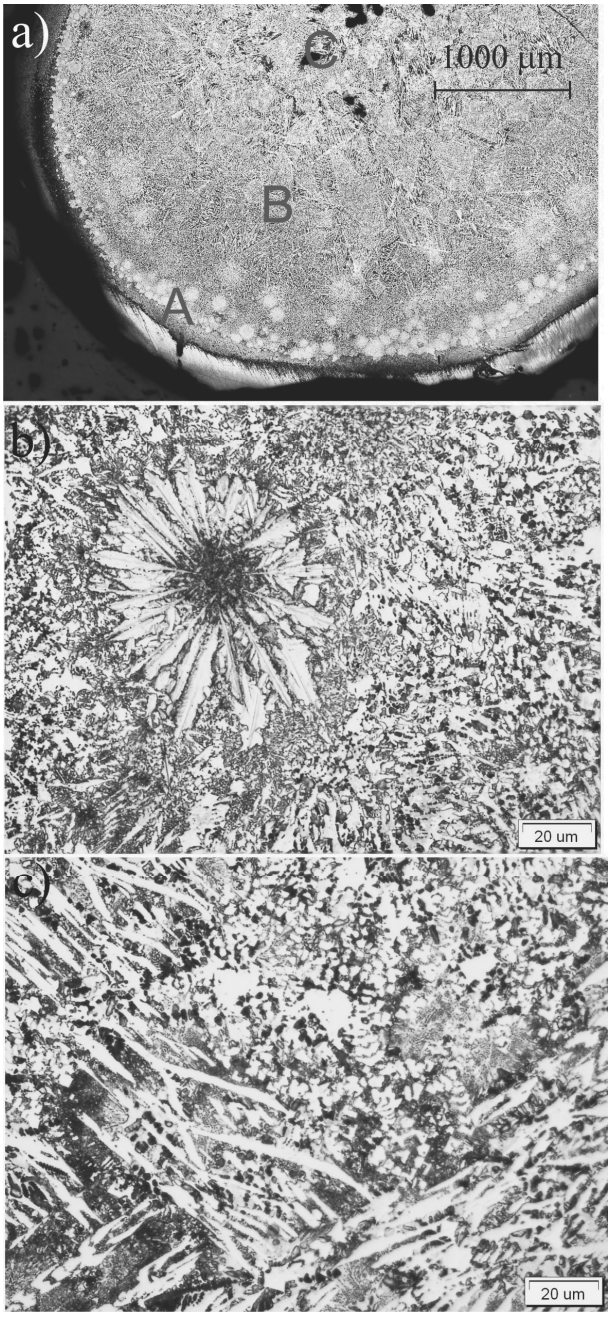

Fig. 10. Optical micrographs of the transverse cross sections after etching of the $Fe_{36}Co_{36}B_{19}Si_5Nb_4$ rods with 5.0 mm in diameter (a-c)

Fan J.T. and Inoue A. noted the quantity of the excess free volume in the structure of $Co_{43}Fe_{20}$ $Ta_{5,5}B_{31,5}$ rods determined by the cooling rate.

The fractures of the cast $Fe_{36}Co_{36}B_{19}Si_5Nb_4$ alloy rods after decohesion in bending test have different character dependent on diameter of rods and regions of investigated (Figs. 14-19).

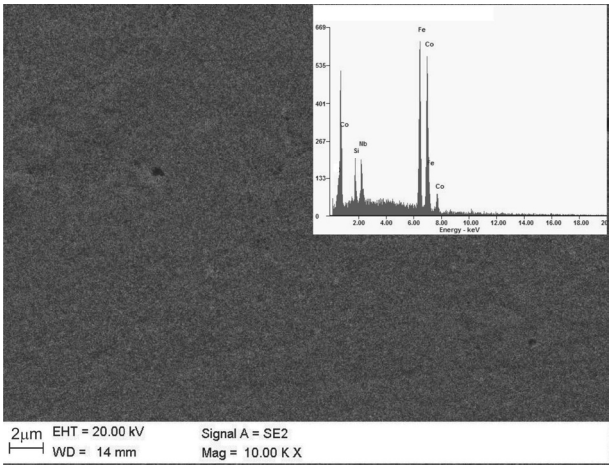

Fig. 11. SEM backscattered electron micrograph of the as-cast rods with 5 mm in diameter on the etched cross-section surface: the image no hint for any visible crystallization phase - amorphous structure

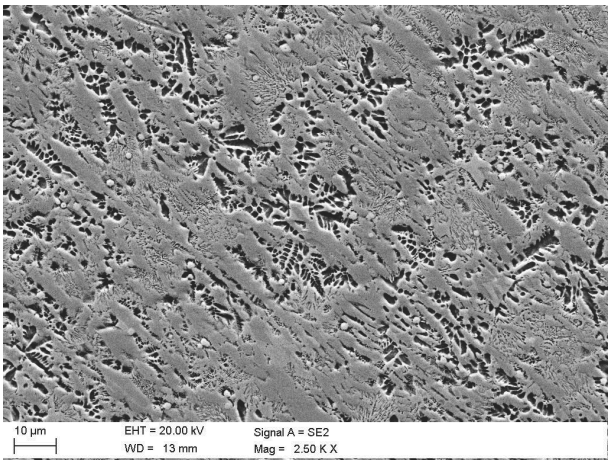

Fig. 12. SEM backscattered electron micrograph of the as-cast rods with 5 mm in diameter on the etched cross-section surface: the dendritic crystalline phases and sphere-form precipitates

Investigations of fractures of the $Fe_{36}Co_{36}B_{19}Si_5Nb_4$ alloy rods with 1.5 and 2.5 mm in diameter (Fig. 14 a,b and Fig. 15 a,b,c, respectively) showed typical morphology of the relaxation amorphous phase. Fracture surface of both, zone having contact with the copper mould during cooling and zone region between surface and core of rod with 1.5 and 2.5 mm in diameter showed the same morphology characterized by smooth fracture with areas of weakly formed vein and chevron pattern morphology. Their character of fracture is typical for the relaxation amorphous materials.

Investigations of fractures of the $Fe_{36}Co_{36}B_{19}Si_5Nb_4$ alloy rods with 3.0 mm in diameter (Fig. 18) showed similar morphology with the exception of central part of rod. In these area contraction cavity was observed and single columnar crystals build up are visible (Fig. 18 c, d).

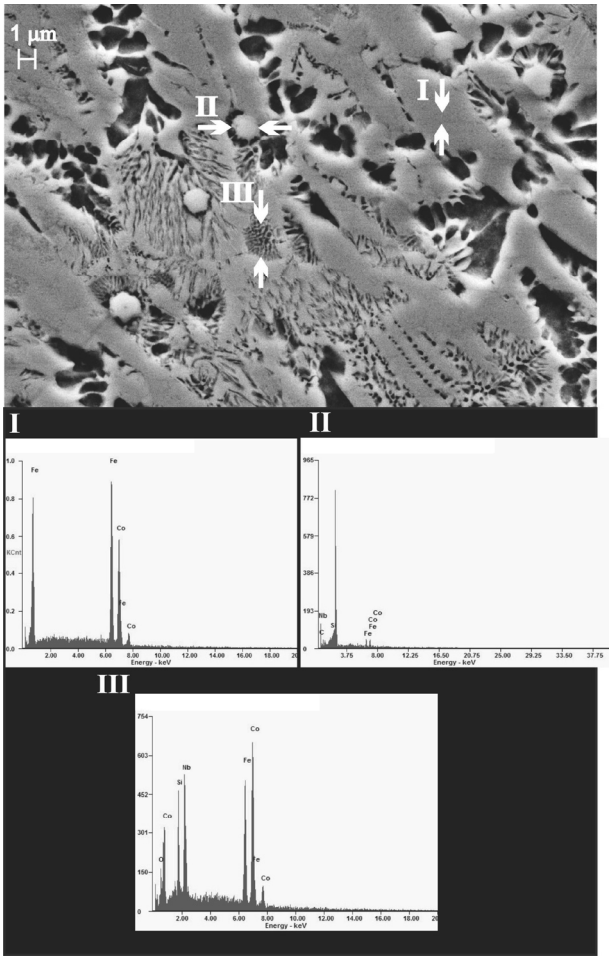

Fig. 13. SEM backscattered electron micrograph of the as-cast rods with 5 mm in diameter on the etched cross-section surface: I, II, III - the place of EDS analysis with results

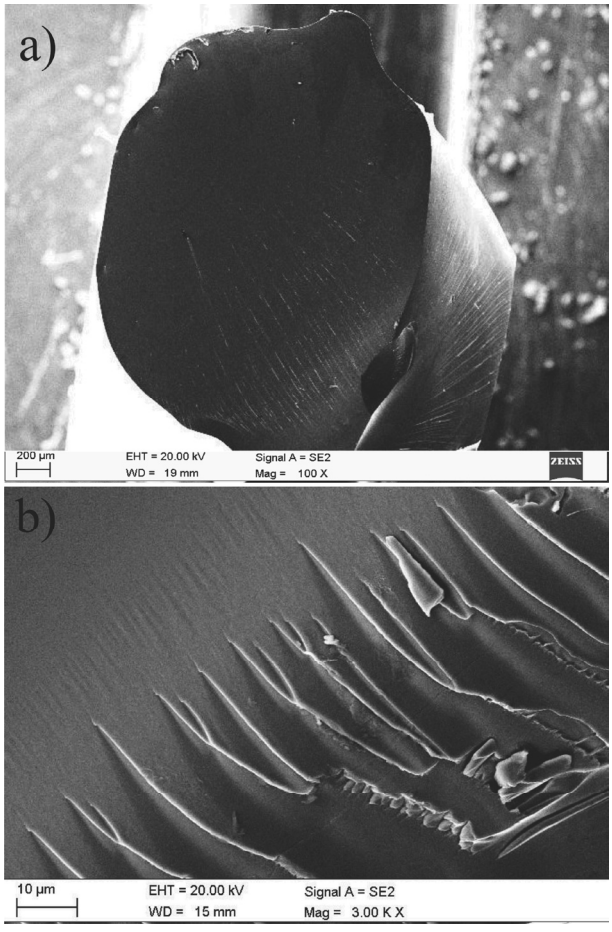

Fig. 14. SEM micrographs of the fracture morphology of $Fe_{36}Co_{36}B_{19}Si_5Nb_4$ rods in as-cast state with diameter of 1.5 mm; a - main view, b - image of fracture outside surface

Fracture morphology in region between surface and core of rod revealed weakly formed fine (shell) chevron pattern morphology, typical for the relaxation metallic glasses (Fig. 18 b). Results of investigations of XRD-method from the cross section of the $Fe_{36}Co_{36}B_{19}Si_5Nb_4$ rods showed existence of crystalline phase besides prevailing amorphous phase in structure of these rod (Fig. 5).

The fractography of the $Fe_{36}Co_{36}B_{19}Si_5Nb_4$ alloy rods with 5.0 mm in diameter (Figs. 19 a-d). showed prevailing smooth fracture with pores and contraction cavity in core of rod (Figs. 19 c, d).

Locally on the surface non-large irregularity of surface corresponding to surface of crystallite distribution with local non-large surface fault have occurred (Fig. 19 b).

In area of central part of rod contraction cavity was observed with columnar crystals freely build up (Fig. 19 c, d).

Results of microhardness measurements point a change of microhardness of as-cast rods dependent on diameter of rods as a result of different relaxation amorphous structure and initiate of crystallization (Figs. 16, 17).

Microhardness varies between 1100-1133 HV on the surface of rods with 1.5 mm in diameter. Similarly, value of microhardness keep at a constant level to distance from the sample's edge about 0.4 mm. However microhardness increase to 1160 HV in core of rod (Fig. 16). These changes of microhardness are probably connected with changes structure relaxation. In core of rod, where cooling rate of rods during casting is lower, the structure is much relaxation. Thus increase of microhardness is due to decay of free volume content (microvoids) proceed at first stage of relaxation process.

Microhardness on the surface of rods with 2.5 mm in diameter to distance from the sample's edge about 1.0 mm is constant and equal 1180 HV, which is correspond to strongly relaxed amorphous structure. However microhardness in core of the rod is equal to 1230 HV and is probably the result of precipitation of hard crystalline phases from amorphous matrix, what causes increase of microhardness (Fig. 16).

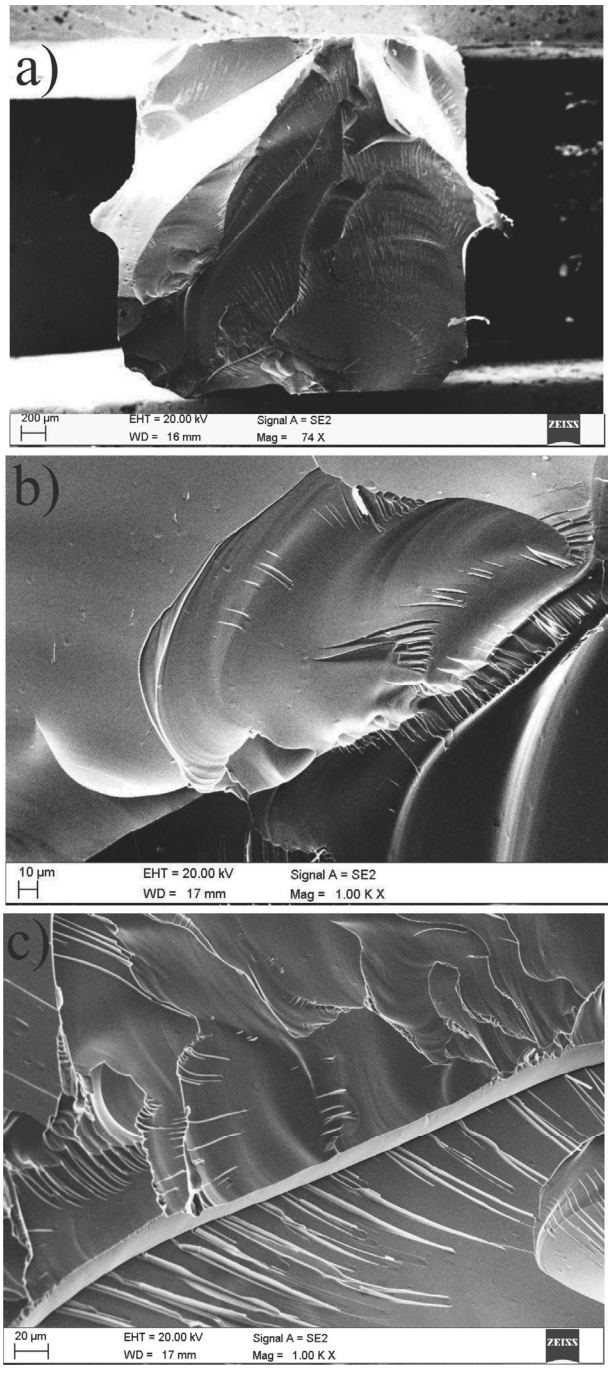

Fig. 15. SEM micrographs of the fracture morphology of $Fe_{36}Co_{36}B_{19}Si_5Nb_4$ rods in as-cast state with diameter of 2.5 mm; a - main view , b and c - image of fracture of core of rod

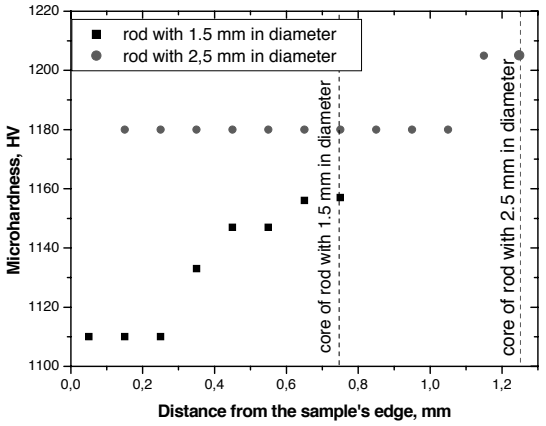

Fig. 16. Results of microhardness experiments of $Fe_{36}Co_{36}B_{19}Si_5Nb_4$ rods with square section 1.5 and 2.5 mm

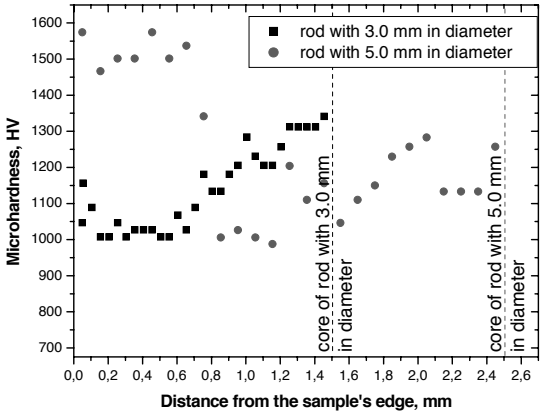

Fig. 17. Results of microhardness experiments of $Fe_{36}Co_{36}B_{19}Si_5Nb_4$ rods with square section 3.0 and 5.0 mm

Results of microhardness experiments on rods with 3.0 and 5.0 mm in diameter, which in core of rods advanced proceed of crystallization is observed, are presented in Fig. 17.

Increase of microhardness to value of ~1300 HV have been observed in core of rods with 3.0 mm in diameter, similar to 2.5 mm in diameter (Fig. 17). It can be pointed out on the structural relaxation process as well as beginning of crystallization process

Significant differences of microhardness on the cross section of rods with 5.0 mm in diameter have been stated. Maximum value of microhardness occur on the surface to distance from the sample's edge about 0.6 mm. Microhardness of zone region between surface and core of rod are decrease and then increase again due to proceed

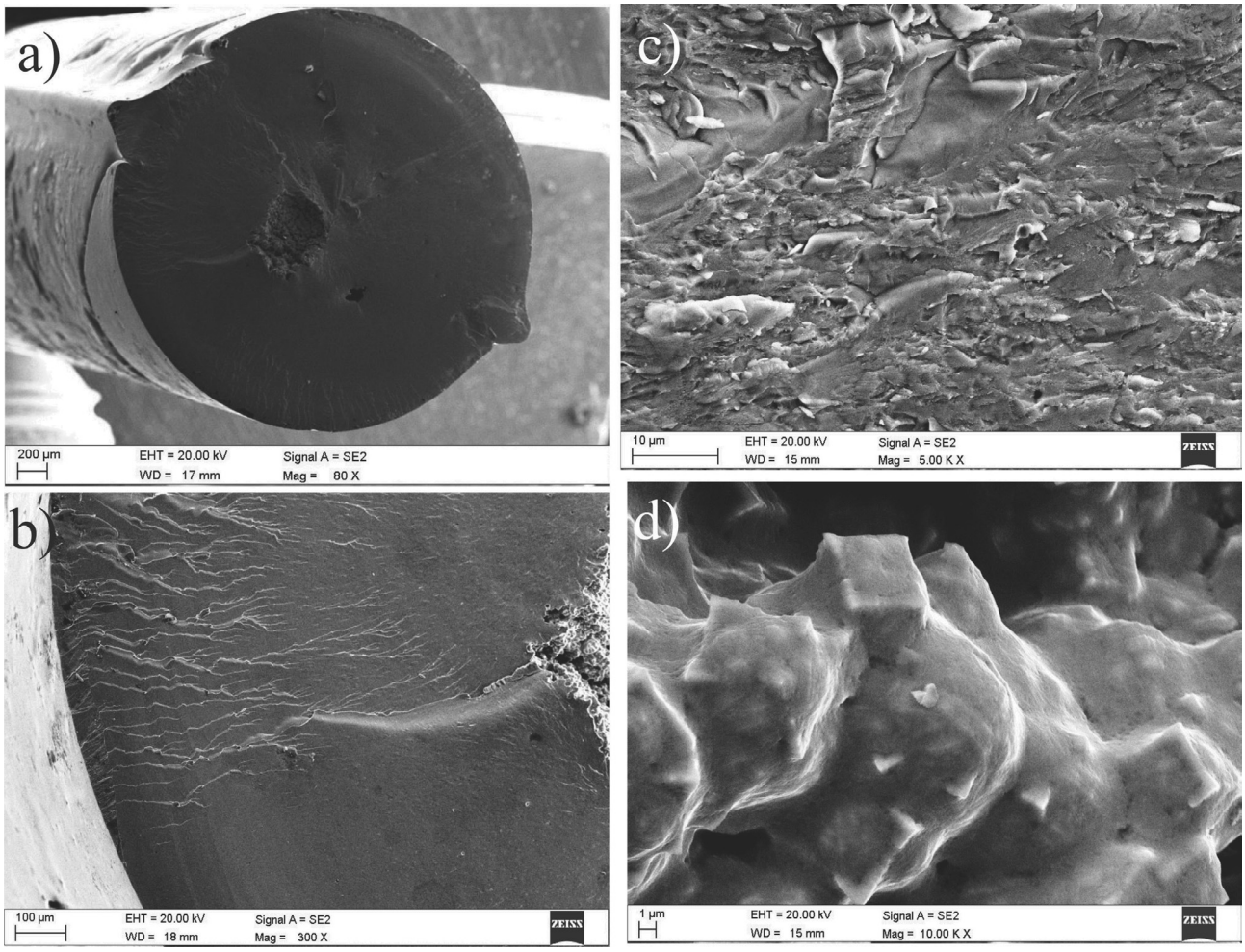

Fig. 18. SEM micrographs of the fracture morphology of $Fe_{36}Co_{36}B_{19}Si_5Nb_4$ rods in as-cast state with diameter of 3.0 mm; a - general view, b - the sample's surface (from A to C - zone, see Fig. 7), c - transition zone (B - zone, see Fig. 7)), d - core, central part of rod in contraction cavity area (C - zone, see Fig. 7)

crystallization process, differences of phase composition and morphology on the cross section of rods (Fig. 17).

The values of microhardness of rods of $Fe_{36}Co_{36}B_{19}Si_5Nb_4$ considerably exceed values obtained for these alloy in rod form (with 5 mm diameter) - 1220 HV in [1].

4. Conclusions

The results obtained are summarized as follows:

- The structure of surface, cross section and powdered materials of rods is different. The surface of rods with diameter of 1,5 i 2,5 and 3.0 mm has amorphous structure. In rods with diameter of 2,5 and 3.0 mm amorphous structure with crystalline phases were observed in further distance from the sample's surface. In zone of surface of rod with diameter of 5.0 mm thin layer of amorphous phase was observed, while in core of rod considerable participation of crystalline phases were present. Rods with diameter of 3.0 mm as well as 5.0 mm may promise extraordinary application potential as gradient materials with different structure on the cross section.
- Fracture morphology of rods have been different on the cross section. Smooth fracture morphology and smooth fracture with areas of vein and chevron pattern morphology have been observed.
- Microhardness of rods changes in the function of the distance from the sample's edge as a result of relaxation and crystallization process of structure.

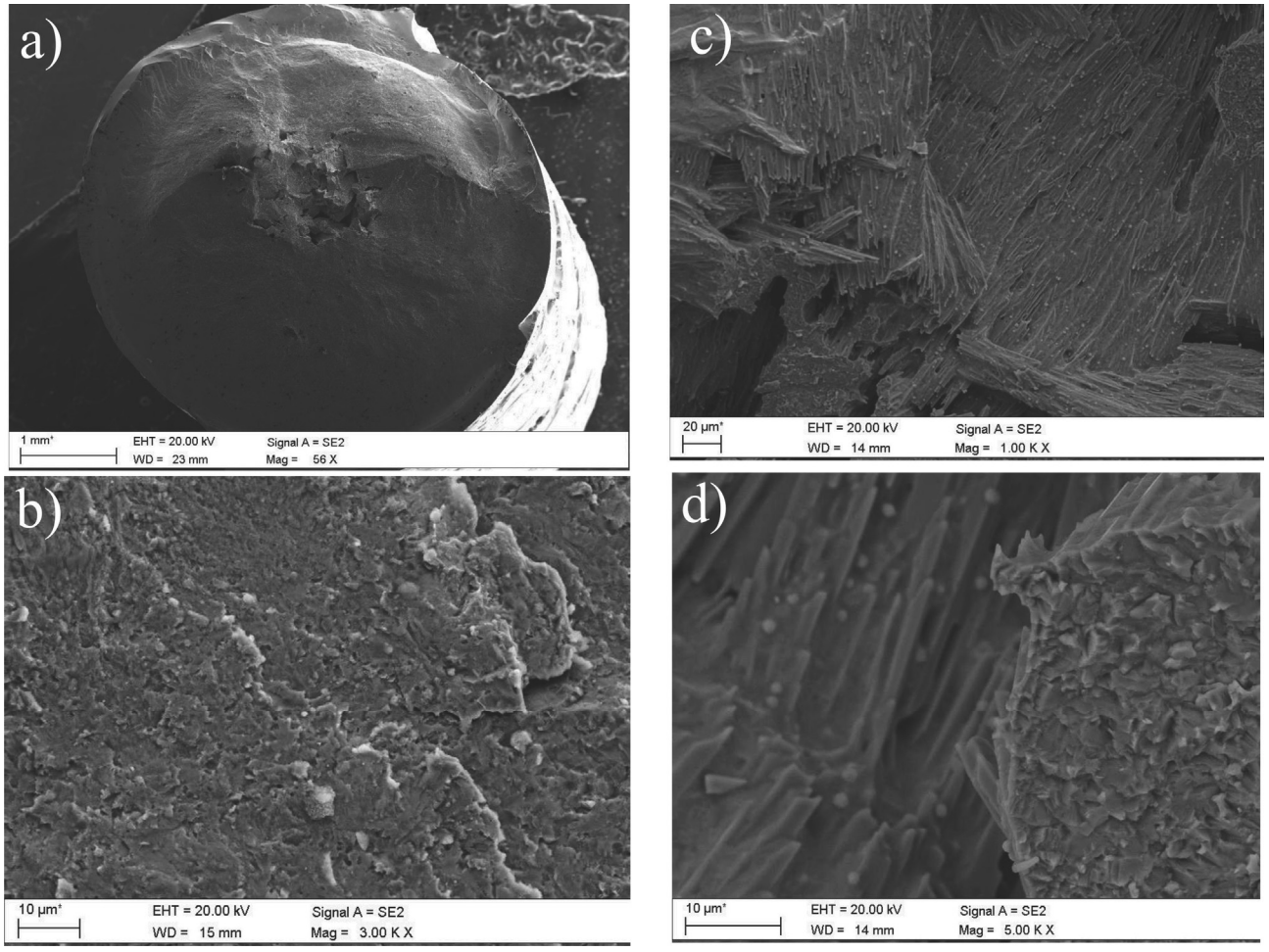

Fig. 19. SEM micrographs of the fracture morphology of $Fe_{36}Co_{36}B_{19}Si_5Nb_4$ rods in as-cast state with diameter of 5.0 mm; a - general view, b - transition zone (B - zone, see Fig. 10), c and d - core, central part of rod in contraction cavity area (C - zone, see Fig. 10)

References

[1] A. Inoue, B.L. Shen, C.T. Chang, Fe - and Co-based bulk glossy alloys with ultrahigh strength of over 4000 MPa, Intermetallics 14 (2006) 936 - 944.

[2] R. Nowosielski, R. Babilas, S. Griner, Z. Stokłosa: Structure and soft magnetic properties of $Fe_{72}B_{20}Si_4Nb_4$ bulk metallic glasses, Archives of Materials Science and Engineering 35/1 (2009) 13-20.

[3] S. Lesz, D. Szewieczek, J. Tyrlik-Held, Correlation between fracture morphology and mechanical properties of NANOPERM alloys, Archives of Materials Science and Engineering 29/2 (2008) 73-80.

[4] B. Shen, A. Inoue, Superhigh strength and good soft-magnetic properties of (Fe,Co)-B-Si-Nb bulk glassy alloys with high glass-forming ability, Applied Physics Letters 85/21 (2004) 4911-4913.

[5] K.F. Yao, C.Q. Zhang, Fe-based bulk metallic glass with high plasticity, Applied Physics Letters 90 (2007) 061901.

[6] S. Lesz, P. Kwapuliński, R. Nowosielski, Formation and physical properties of Fe-based bulk metallic glasses with Ni addition, Journal of Achievements in Materials and Manufacturing Engineering 31/1 (2008) 35-40.

[7] S. Lesz , Z. Stokłosa, R. Nowosielski, Influence of copper addition on properties of $(Fe_{36}Co_{36}B_{19}Si_5Nb_4)_{100-x}Cu_x$ metallic glasses, Archives of Materials Science and Engineering 38/1 (2009) 12-18.

[8] R. Nowosielski, R. Babilas, Structure and magnetic properties of $Fe_{36}Co_{36}B_{19}Si_5Nb_4$ bulk metallic glasses, Journal of Achievements in Materials and Manufacturing Engineering 30/2 (2008) 135-140.

[9] Z.H. Gan, H.Y. Yi, J. Pu, J.F. Wang, J.Z. Xiao, Preparation of bulk amorphous Fe-Ni-P-B-Ga alloys from industrial raw materials, Scripta Materialia 48 (2003) 1543-1547.

[10] A. Makino, T. Kubota, C. Chang, M. Makabe, A. Inoue, FeSiBP bulk metallic glasses with high magnetization and excellent magnetic softness, Journal of Magnetism and Magnetic Materials 320 (2008) 2499-2503.
[11] A. Makino, C. Chang, T. Kubota, A. Inoue, Soft magnetic Fe-Si-B-P-C bulk metallic glasses without any glass-forming metal elements, Journal of Alloys and Compounds 483 (2009) 616-619.
[12] A.R. Pierna, A. Lorenzo, F.F. Marzo, A. Altube, M. Sistiaga, Electrochemical behaviour of $Fe_{40}Ni_{38}Mo_4B_{18}$ amorphous alloys in aqueous solution at high pH. Influence of the structural relaxation, Journal of Non-Crystalline Solids 235-237 (1998) 796-799.
[13] Q. Jing, R.P. Liu, G. Li , W.K. Wang, Thermal expansion behavior and structure relaxation of ZrTiCuNiBe bulk amorphous alloy, Scripta Materialia 49 (2003) 111-115.
[14] PN - EN ISO 6507 - 1:2007.
[15] W.J. Boettinger, U.R. Kattner, K.-W. Moon, J.H. Perepezko, DTA and Heat flux DSC Measurements of Alloy Melting and Freezing, National Institute of Standards and Technology Special Publication 960-15 (2006).
[16] A. Inoue, A. Takeuchi, T. Zhang: Ferromagnetic Bulk Amorphous Alloys, Metallurgical and Materials Transactions A 29 (1998) 1779-1793.
[17] J.T. Fan, Z.F. Zhang, S.X. Mao, B.L. Shen, A. Inoue, Deformation and fracture behaviors of Co-based metallic glass and its composite with dendrites, Intermetallics 17 (2009) 445-452.